Boundary-Layer Meteorol (2008) 128:173–189
DOI 10.1007/s10546-008-9281-2

ORIGINAL PAPER

Effects of Roll Vortices on Turbulent Fluxes in the Hurricane Boundary Layer

Jun A. Zhang · Kristina B. Katsaros · Peter G. Black · Susanne Lehner · Jeffrey R. French · William M. Drennan

Received: 11 February 2008 / Accepted: 26 May 2008 / Published online: 24 June 2008

Abstract Boundary-layer secondary circulations or 'roll vortices' can have a significant influence on the turbulent exchange of momentum, sensible heat and moisture throughout the hurricane boundary layer. In this study, analyses of data from a WP-3D aircraft of the National Oceanic and Atmospheric Administration (NOAA) are presented. As part of the Coupled

J. A. Zhang · W. M. Drennan (✉)
Rosenstiel School of Marine and Atmospheric Science, Division of Applied Marine Physics, University of Miami, Miami, FL, USA
e-mail: wdrennan@rsmas.miami.edu

Present Address:
J. A. Zhang
Hurricane Research Division, National Oceanographic and Atmospheric Administration (NOAA), Atlantic Oceanographic and Meteorological Laboratory (AOML), Miami, FL, USA

K. B. Katsaros
National Oceanographic and Atmospheric Administration (NOAA), Atlantic Oceanographic and Meteorological Laboratory (AOML), Miami, FL, USA

Present Address:
K. B. Katsaros
P.O. Box 772, Freeland, WA 98249, USA

P. G. Black
Hurricane Research Division, National Oceanographic and Atmospheric Administration (NOAA), Atlantic Oceanographic and Meteorological Laboratory (AOML), Miami, FL, USA

Present Address:
P. G. Black
Science Applications International Corporation at Naval Research Laboratory, Monterey, CA, USA

S. Lehner
German Aerospace Centre (DLR), Oberpfaffenhofen, Germany

J. R. French
Department of Atmospheric Science, University of Wyoming, Laramie, WY, USA

Boundary Layer Air-Sea Transfer (CBLAST)-hurricane experiment sponsored through the Office of Naval Research and NOAA's annual hurricane research program, flights were conducted to investigate energy exchange across the air–sea interface. We present the first in-situ aircraft-based observations of rolls in the hurricane boundary layer and investigate their influence on energy and momentum exchange. The rolls detected in Hurricane Isidore (year 2002) have a characteristic wavelength of about 900 m, in good agreement with analyses of data from a synthetic aperture radar image captured by the Canadian Space Agency's RADARSAT satellite in the same storm. Our analyses of the airborne data suggest that roll vortices may be a significant factor modulating the air–sea momentum exchange.

Keywords Air–sea interaction · Hurricane boundary layer · Roll vortices · Turbulent fluxes

1 Introduction

Roll vortices in the atmospheric boundary layer (ABL) have been investigated in previous theoretical and field studies (e.g., LeMone 1973; Brown 1970; Glendening 1996; Weckwerth et al. 1997); for reference also see the review articles of Brown (1980), Etling and Brown (1993) and Young et al. (2002). Depending on their size and strength, roll vortices have the potential to play a significant role in transporting momentum, heat and moisture through the atmospheric boundary layer. Failing to adequately sample these coherent structures could easily lead to an underestimation or overestimation of boundary-layer fluxes. Recent remote sensing observations show that roll vortices may be common in the hurricane boundary layer (HBL) (Morrison et al. 2005).

Synthetic Aperture Radar (SAR) can provide useful information for identifying atmospheric mesoscale variations, such as ABL rolls (Alpers and Brümmer 1994; Mourad 1996; Mourad and Walter 1996; Brümmer 1999; Müller et al. 1999; Levy and Brown 1998). The coherent structures of rolls can cause distinctive alteration of the ocean surface roughness on scales $\sim$10 mm that are sensed by SAR via the change of the Bragg wave spectrum. Katsaros et al. (2000) report on the examination of several RADARSAT SAR images from four hurricanes (Bonnie, Danielle, Georges, and Mitch) in 1998 as part of a program sponsored by the Canadian Space Agency. In addition to the identification of numerous effects of rain and convective rainbands, they also recognized features they attributed to roll vortices in the ABL in regions between rainbands. By examining SAR images of Hurricanes Mitch and Floyd, Katsaros et al. (2002) found similar periodic variation in sea surface roughness as that induced by roll vortices, and speculate that such features may be endemic to hurricane surface flows over the ocean. Some aspects of SAR-observed coherent roll-scale features are also discussed by Vachon and Katsaros (1999) and Friedman et al. (2004).

Intense sub-km-scale rolls in the HBL have been inferred from mobile Doppler radar (Wurman and Winslow 1998). Morrison et al. (2005) used National Weather Service WSR-88D fixed coastal Doppler radars to show that roll vortices occur in 35–69% of the radar volumes of four hurricane landfalls with mean roll wavelengths of 1450 m, aspect ratio of 2.4, and azimuthal wind variations of about 7 m s^{-1}. They also suggest that the HBL fluxes are 2–3 times greater than estimated by parameterizations in numerical weather prediction models due to the presence of such rolls. Recently, Lorsolo et al. (2008) analysed the data from the Shared Mobile Atmospheric Research and Teaching (SMART) radars in the HBL and found that the wavelengths of the majority of rolls that are omnipresent in their data are between 200 and 650 m in agreement with Wurman and Winslow (1998).

Foster (2005) has recently developed a theory for roll vortices in curved flow at high wind speeds, such as in hurricanes, suggesting that HBL rolls transport high-momentum air from the upper HBL downward (and low-momentum air from the lower HBL upward) and enhance air–sea exchange. Nolan (2005) investigated the mechanisms for rolls in the hurricane boundary layer using numerical simulations and analyses of idealized vortices, and showed that an instability associated with the inflection points of the swirling boundary layer in hurricanes is a good candidate mechanism for the appearance of secondary circulations, although it is unclear whether these are the same features as those discussed herein.

ABL rolls have also been investigated using research aircraft (LeMone 1976; Chou and Ferguson 1991; Brooks and Rogers 1997; Chen et al. 2001; Vandemark et al. 2001) and from tower-based anemometer observations (Savtchenko 1999). However, to date no such measurements have been made in the HBL.

Here we report the first in-situ turbulent flux measurements with near-coincident SAR imagery in the presence of rolls in the HBL. The main purpose of this study is to investigate the significance of roll vortices on the exchange of energy across the air–sea interface and within the HBL. A brief description of the experiment is presented in the following section. Section 3 describes the satellite data employed and the analysis of a RADARSAT-1 SAR image captured near the area of the boundary-layer aircraft measurements during Hurricane Isidore (year 2002). Section 4 discusses the turbulent flux and secondary-flow analyses in this storm, and finally, we provide discussion and summary in Sect. 5.

2 Experiment Description

Prior to the 2002 hurricane season, the "Hurricane Watch" program was established by the Canadian Space Agency (CSA) and Canadian Centre for Remote Sensing (CCRS) in collaboration with the National Oceanic and Atmospheric Administration (NOAA) Hurricane Research Division (HRD) flight planning team and the NOAA Aircraft Operations Center (AOC). In this program, numerous RADARSAT SAR images were obtained in and around hurricanes during the 2002 and 2003 seasons. Concurrently, the Office of Naval Research (ONR) sponsored Coupled Boundary Layer Air-Sea Transfer (CBLAST) experiment had its major hurricane field measurement campaigns. This occurred in conjunction with HRD's Hurricane Field Program during the Atlantic hurricane seasons of 2002–2004. A summary of the CBLAST-hurricane experiment is given in Black et al. (2007).

As part of CBLAST, boundary-layer observations were made using NOAA's specially instrumented WP-3D Orion aircraft (hereafter referred to by its call sign, NOAA43, referring to its tail number, N43RF). Typical CBLAST flights lasted about 8 h and included transit, calibration, eyewall penetrations, and, in some instances, low-level boundary-layer legs. During the 2002–2003 hurricane seasons, low-level flight legs were used specifically to investigate turbulence and energy fluxes in the HBL. The flight patterns included along-wind and cross-wind stepped descents down to 70 m conducted in clear air regions between rainbands. Details of the flight patterns related to storm position and motion are discussed in Drennan et al. (2007) and Black et al. (2007). Data and measurements of momentum and humidity fluxes during Hurricanes Fabian and Isabel in 2003 are discussed in French et al. (2007) and Drennan et al. (2007), respectively.

The measurements of HBL rolls used in this study are a subset of the data collected during the CBLAST experiment from boundary-layer flight legs in Hurricane Isidore (2002). Flight-level data include winds, temperature, and dew-point temperature, with wind velocity data derived from a fuselage-mounted Rosemount gust probe system, a description of which,

including details of the calibration procedures, is given in French et al. (2007). Humidity data are provided by a low response (<1 Hz) chilled-mirror dewpoint hygrometer (General Eastern 1011), and fast response temperature data are measured using Rosemount 102a sensors (Friehe and Khelif 1992; Khelif et al. 1999). The near-surface neutral-stability wind speed is obtained from a nadir-pointing stepped frequency microwave radiometer (SFMR) (Uhlhorn et al. 2007). Sea-surface temperature (SST) is measured by a Barnes PRT-5 infrared radiometer. In addition, data from GPS (global positioning system) dropsondes provide vertical profiles of potential temperature and specific humidity.

3 RADARSAT-1 SAR Observations

Spaceborne SAR is capable of providing a comprehensive view of the sea surface roughness at a resolution on the order of 10–100 m. Roughness is in part related to the wind speed and thus, from the calibrated radar backscatter, the incidence angle and the wind direction, the wind speed can be derived from the SAR image. Some streak patterns in sea surface roughness can be explained by changes in surface wind speed due to the formation of boundary-layer rolls (Mourad et al. 2000; Sikora and Ufermann 2004). This section briefly describes a RADARSAT-1 image collected in the region of the boundary-layer aircraft measurements in Hurricane Isidore (2002).

Tropical Storm Isidore was upgraded from a tropical depression (TD9) at 0600 UTC, 18 September 2002, near Jamaica (Pasch et al. 2004), and further upgraded to a hurricane 36 h later, and made landfall in western Cuba at 2000 UTC, 20 September 2002 as a category 1 storm. Hurricane Isidore continued westward after passing over Cuba, and strengthened, maintaining category 3 status until making landfall on the Yucatan Peninsula around 2000 UTC, 22 September 2002. The storm centre remained over the Yucatan for the next 36 h during which time the storm gradually weakened. Isidore re-emerged over the Gulf of Mexico late on 24 September as a tropical storm and made landfall again south of New Orleans two days later. The track of Isidore, superimposed on a NOAA-16 AVHRR (Advanced Very High Resolution Radiometer) image from 22 September is shown in Fig. 1.

A RADARSAT-1 SAR image over Hurricane Isidore was acquired by the CSA at 2357 UTC, 23 September 2002, when the storm centre was nearly stationary over the Yucatan (Fig. 2). The RADARSAT-1 SAR is an HH-polarized (horizontal electric field vector orientation for transmit and receive functions) C band (5.3 GHz) radar with nominal spatial resolution of 32 and 20 m in the azimuth and range dimensions, respectively (Vachon and Katsaros 1999). For the purpose of this study, the image was precision-processed after it was calibrated and corrected for power loss (Laur et al. 1998). Detailed algorithms for the analysis of the image are described in Lehner et al. (1998, 2000). The image was first split into subscenes of 20 km (256 pixels of 50 m length and width), and a two-dimensional fast Fourier transform (2D-FFT) algorithm was then used to calculate the directional image spectra for each subscene. In subscenes for which the maximum of the 2D spectrum is due to wind streaks or rolls, the direction of the rolls can be taken to be the wind direction. Image pixels corresponding to land and some types of non-wind features are identified using the algorithm of Koch (2004). While up to this point the algorithm is standard for wind field determination from SAR imagery, we measure additionally the wavelength of the rolls.

Figure 3 shows the analysis result of the SAR image. While earlier studies have investigated SAR images of hurricanes to derive wind speed (Horstmann et al. 2005) and others to determine sea state (Li et al. 2002), here we concentrate on the roll structures in the image such as that shown in Fig. 2c. The upper left panel of Fig. 3 shows the wavelength and

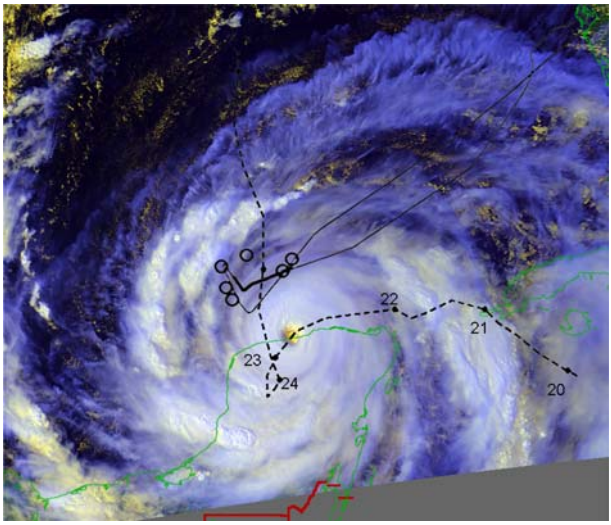

Fig. 1 NOAA43 aircraft track (*solid black line*) on top of the NOAA-16 AVHRR image at 1958 UTC, on 22 September 2002. Image © 2002 by the Ocean Remote Sensing Group at Johns Hopkins University Applied Physics Laboratory. The dashed line shows the track of Hurricane Isidore from 20 to 26 September 2002 with positions indicated by dots at 0000 UTC. Also shown are the release locations (◯) of the dropsondes of Fig. 4

direction of the wind streaks, and the upper right panel of Fig. 3 shows the histogram of the wavelengths of the rolls for the entire image with a maximum in the distribution of about 900 m. The lower two panels in Fig. 3 demonstrate the analyses of the two boxes of interest indicated in Fig. 2. The wavelengths of the rolls in these two boxes vary from around 400 to 1100 m, which illustrates how the scales vary within a storm.

4 Aircraft Observations

NOAA43 conducted missions into Isidore on 21, 22 and 25 September 2002, and of interest here is the NOAA43 flight late on 22 September that occurred roughly 24 h prior to the SAR overpass discussed in the previous section. Throughout this period the hurricane eye was situated at the northern edge of the Yucatan Peninsula as shown in Fig. 1. Boundary-layer profiles of potential temperature and specific humidity retrieved from GPS dropsondes released in the vicinity of the boundary-layer leg are shown in Fig. 4. Boundary-layer height was estimated from the potential temperature profiles (following Stull 1988) to be around 500 m. The dropsondes were qualitatively selected based on their proximity to the aircraft flight track, both spatially and temporally; the flight track along with dropsonde release positions are shown in Fig. 1.

Figure 5 presents data from that portion of the flight between 2210 and 2240 UTC. Flight level parameters of interest include aircraft altitude, wind speed, wind direction, and aircraft attitude angles. In Fig. 5b, the black lines below the altitude plots represent the times of the five flux run legs, denoted by A–E for reference hereafter. Flux run A is the nearly cross-wind leg, while B, C and D are nearly along-wind legs. Leg E is a transverse leg with an angle of around 40° between the aircraft ground track and the mean wind direction. Aircraft altitude

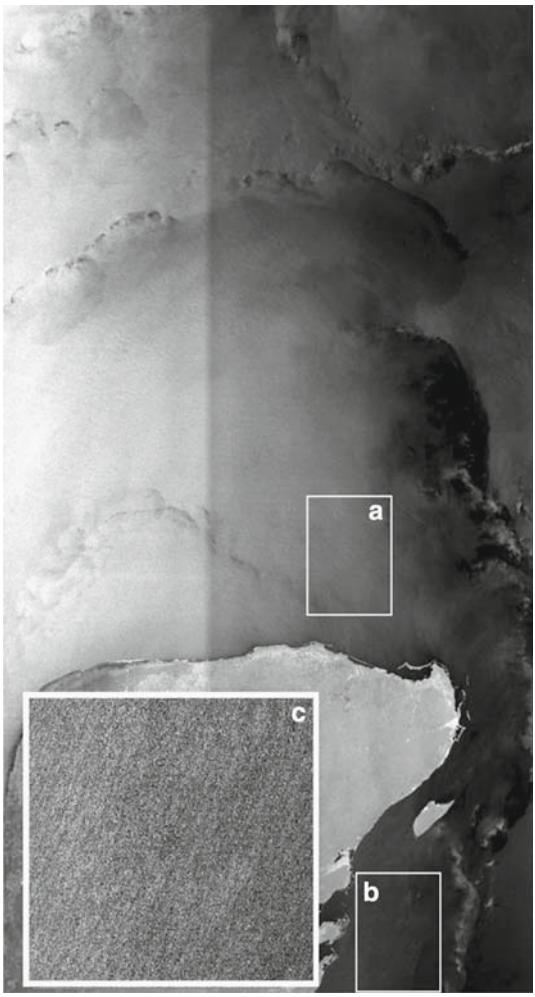

Fig. 2 RADARSAT-1 SAR image of Hurricane Isidore acquired on 23 September 2002 at 2357 UTC after landfall on the Yucatan Peninsula. Image © Canadian Space Agency. Analyses of this image and the two boxes (a and b) are shown in Fig. 3. Subimage c shows a 38×45 km high-resolution subimage from region b

and attitude angles (pitch, roll and heading) were checked and confined to a specific range during each leg in order to reduce the spurious values in the wind measurements caused by the sudden changes of these quantities. The entire low-level portion of this flight leg was confined to 200 and 350 m altitude and hence is within the HBL at all times.

All flux measurements were taken between rainbands well outside of the eyewall. The thermodynamic conditions of the HBL were near neutral to slightly unstable. The stability parameter, z/L, is shown in Table 1, where z is the aircraft altitude and L is the Obukhov length calculated using an iterative method (Drennan and Shay 2006). Previous theoretical and numerical studies suggest that this atmospheric environment is favourable to the formation of roll vortices (Lilly 1966; Brown 1980; Young et al. 2002; Foster 2005).

The aircraft-measured wind vector was rotated into its along-wind (u) and cross-wind (v) components before analysis, and the three components of the wind velocity, potential temperature and humidity were then detrended to derive the turbulent fluctuations. Figure 6 shows time series of the turbulent fluctuations of the wind velocity vector (u', v' and w'),

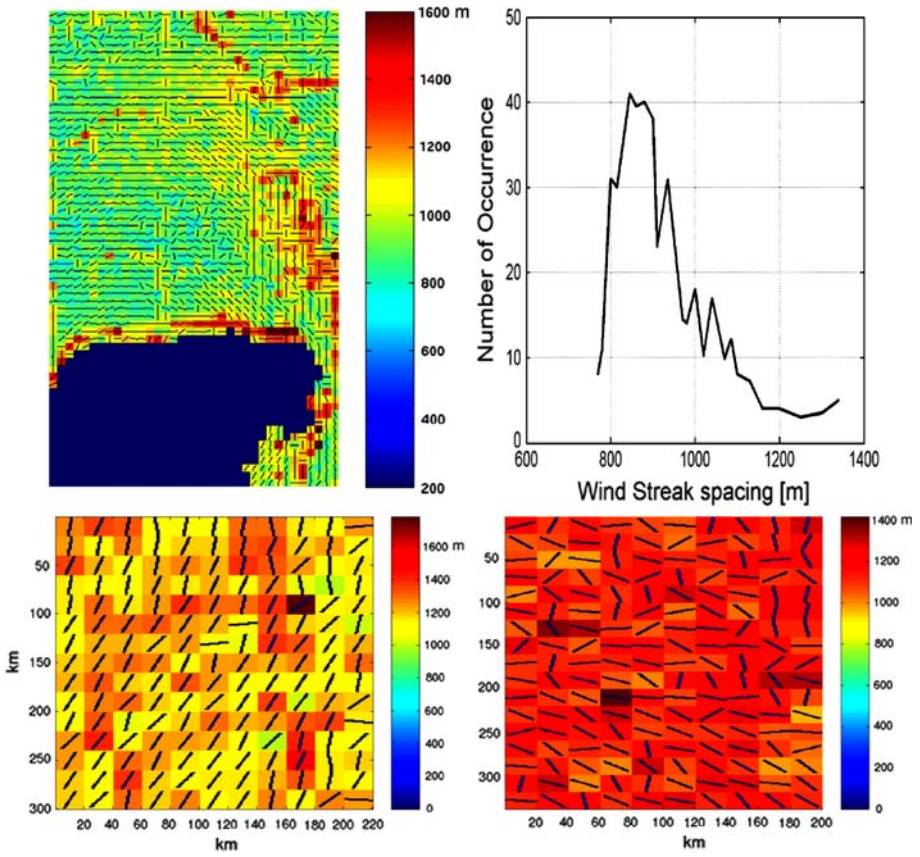

Fig. 3 Analysis result of the SAR image in Fig. 2. The upper left panel shows the wavelength (colour bar code, m) and direction of the wind rolls. The upper right panel shows the histogram of the roll wavelengths of the entire image at left. The lower two (left/right) panels show the wavelength and direction analysis of the boxes (b/a) in Fig. 2

potential temperature (θ') and absolute humidity (q'), along with the product terms ($w'\theta'$ and $w'q'$) for the cross-wind leg (A). Note that all the above variables except q are sampled at 40 Hz, although only 1 Hz data are shown here.

Figure 7 shows the frequency-weighted power spectral density of u', v', w', θ', and q' for the cross-wind leg (A), where there are significant peaks in the spectral plots of all the variables at 0.13 Hz. Given the true airspeed of 110 m s^{-1} and accounting for the 80° track angle relative to the wind, this would be equivalent to a wavelength ≈900 m. A number of small peaks between 0.3 and 1 Hz (330 and 100 m), which also appear in the spectra of u',v',w' and θ', can be related to the smaller-scale plumes and less organized turbulence. There is no smaller-scale turbulence signal above 0.5 Hz in the power spectra of q' due to the lack of a fast response humidity sensor during the 2002 measurements. Note that Drennan et al. (2007) showed the humidity signal from the chilled-mirror hygrometer agreed well with the signal from the faster response infrared hygrometer available after 2002 for frequencies below about 0.3 Hz.

To confirm the presence of rolls during the aircraft measurements, a Morlet wavelet transform (Grossmann and Morlet 1984) was applied to the vertical velocity signals. A wavelet

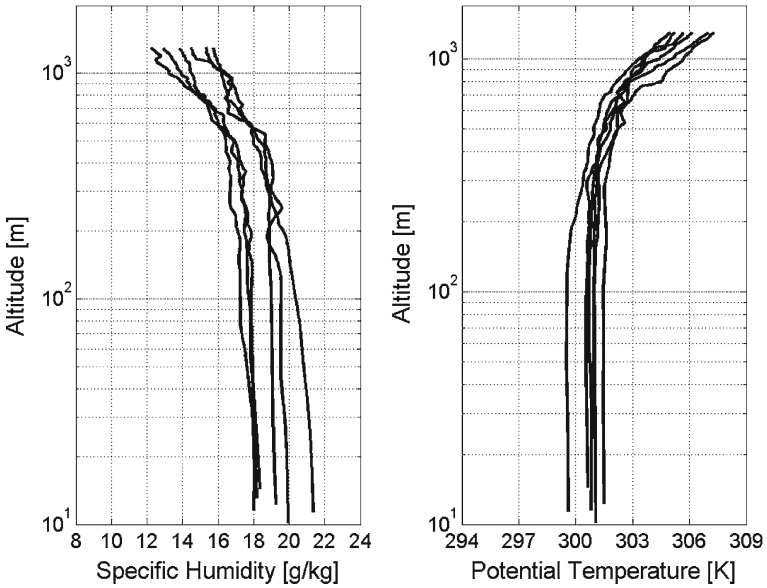

Fig. 4 Specific humidity (left) and potential temperature (right) from six GPS dropsondes dropped from NOAA43 in the vicinity of the 22 September 2002 boundary-layer flight. The release points of the sondes are shown in Fig. 1

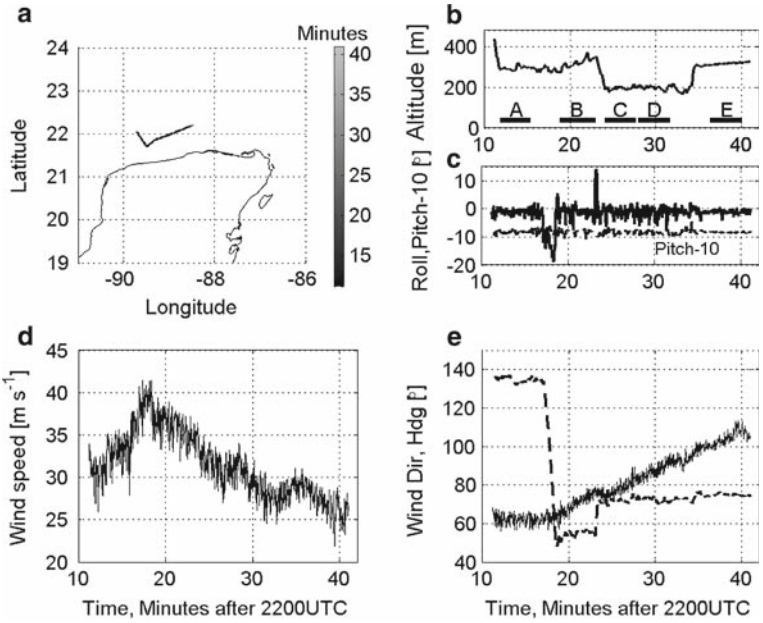

Fig. 5 NOAA43 flight track (**a**) during Hurricane Isidore on 22 September 2002, 2210-2242 UTC. Also shown are the aircraft altitude (**b**), pitch and roll (**c**), wind speed (**d**), and aircraft heading (*dashed*) and wind (*solid*) directions (**e**). In panel b the five black lines denoted A – E indicate the flux runs

Table 1 Summary of data and calculations for the five flux run legs (A, B, C, D and E) in Hurricane Isidore on 22 September 2002

Leg	Leg time UTC	Leg length (km)	Leg type	z (m)	U_z (m s^{-1})	U_{10N} (m s^{-1})	z/L	u_* (m s^{-1})	$C_{D10N}(\times 10^3)$	θ_{10} (K)	SST (K)	$\langle\theta' w'\rangle$ (K m s^{-1})
A	2211–2215	24.6	cross	293	32.4	21.6	−0.001	1.08	2.51	301.5	300.4	0.028
B	2218–2222	24.5	along	319	35.3	23.0	−0.023	1.04	2.06	301.7	300.4	0.037
C	2223–2227	24.3	along	194	30.2	21.1	−0.017	0.98	2.17	301.5	300.3	0.036
D	2227–2231	24.4	along	196	29.1	20.3	−0.023	0.88	1.89	301.7	300.3	0.025
E	2236–2239	24.3	along	315	28.8	18.1	−0.023	0.81	2.05	301.4	300.2	0.022

The variables are altitude (z), flight level wind speed (U_z), neutral 10 m wind speed (U_{10N}), stability (where L is the Obukhov length), surface friction velocity (u_*), neutral 10-m drag coefficient (C_{D10N}), neutral 10-m potential temperature (θ_{10}), sea surface temperature (SST) and covariance heat flux ($\theta' w'$)

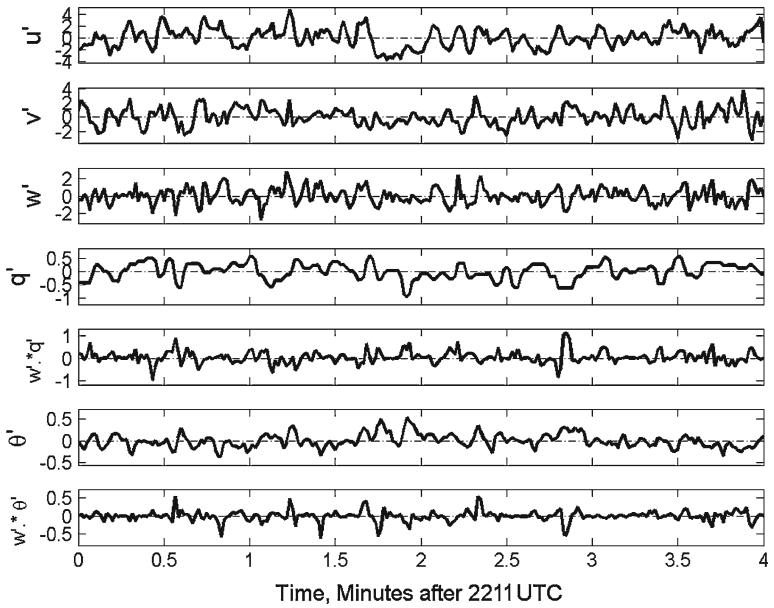

Fig. 6 Data from cross-wind leg A, showing time series of the fluctuations of the three components of wind velocity (horizontal along-wind u, horizontal cross-wind v, and vertical w), absolute humidity, and potential temperature, along with product terms $w'q'$ and $w'\theta'$

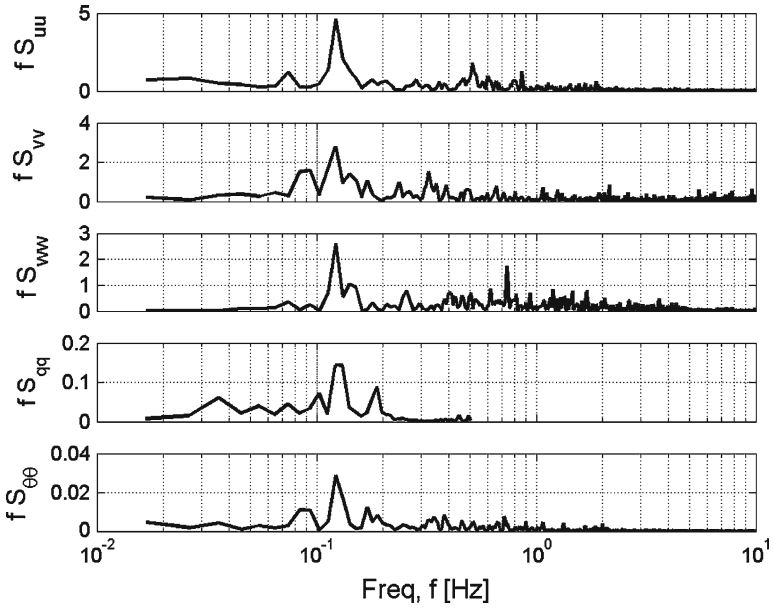

Fig. 7 Data from cross-wind leg A, showing spectra of three velocity components (horizontal along-wind u; horizontal cross-wind v and vertical w), humidity and potential temperature

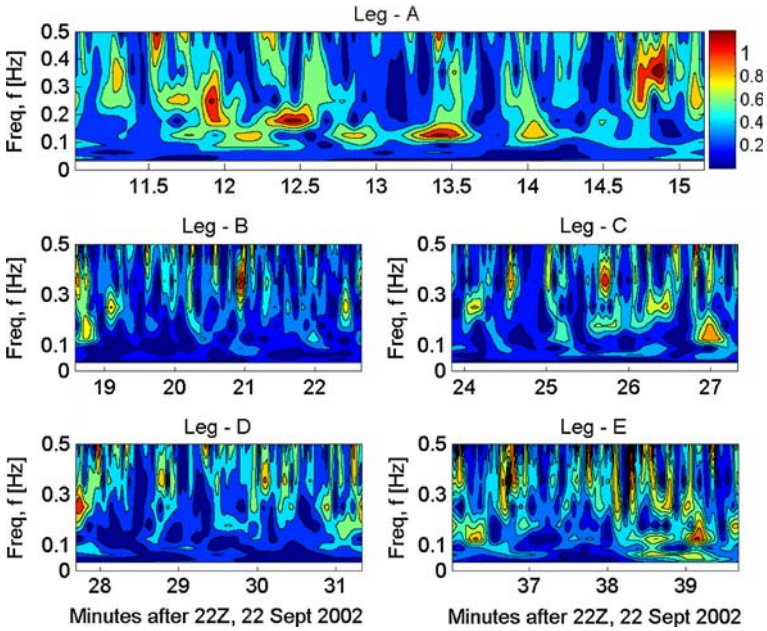

Fig. 8 Contour plots of wavelet coefficient amplitude of the vertical velocity against time and frequency. The five sections (A–E) of the boundary-layer flux run on 22 September 2002 into Hurricane Isabel were analysed separately

transform allows for the decomposition of a signal in both frequency and time domain and hence can be used to study the evolution of features (e.g., Farge 1992). Figure 8 shows the amplitude squared (i.e., energy) of the wavelet coefficients for the five flux run legs. Note the enhanced energy patterns in the wavelet plot during the cross-wind flight leg (A) in the frequency band around 0.13 Hz, corresponding to length scales of 900 m, consistent with the features seen in the SAR images discussed in the previous section. That such coherent features are only infrequently observed in the subsequent near-along-wind and transverse legs, is consistent with the identification of these features as roll vortices. The rolls are generally lined-up in the wind direction (i.e., Young et al. 2002; Morrison et al. 2005; Foster 2005), so would be expected to be less frequently encountered in flight legs along the wind direction.

From the detrended turbulent signals, we calculate the along-wind and cross-wind components to the stress, $-\overline{u'w'}$ and $-\overline{v'w'}$, along with $\overline{\theta'w'}$ and $\overline{q'w'}$, and the surface friction velocity $\left(u_* = \left[\overline{-u'w'}^2 + \overline{-v'w'}^2\right]^{1/4}_{sfc}\right)$ is estimated following the method described in French et al. (2007). The influence of the Coriolis force and the horizontal pressure gradient is included following Donelan (1990). The 10-m neutral drag coefficient, given in Table 1, is calculated using the friction velocity and 10-m wind speed using $C_{D10N} = u_*^2/U_{10N}^2$.

Table 1 summarizes the measurements and calculations for each of the five runs; leg-averaged mean flight-level wind speeds vary from 29 to 35 m s^{-1}. The near-surface neutral-stability wind speeds (U_{10N}), determined from measurements by the SFMR, vary from 18 to 23 m s^{-1}. The SST during the flux measurements is nearly uniform implying that the underlying instability conditions are similar for all the five flux runs. Note that corrections

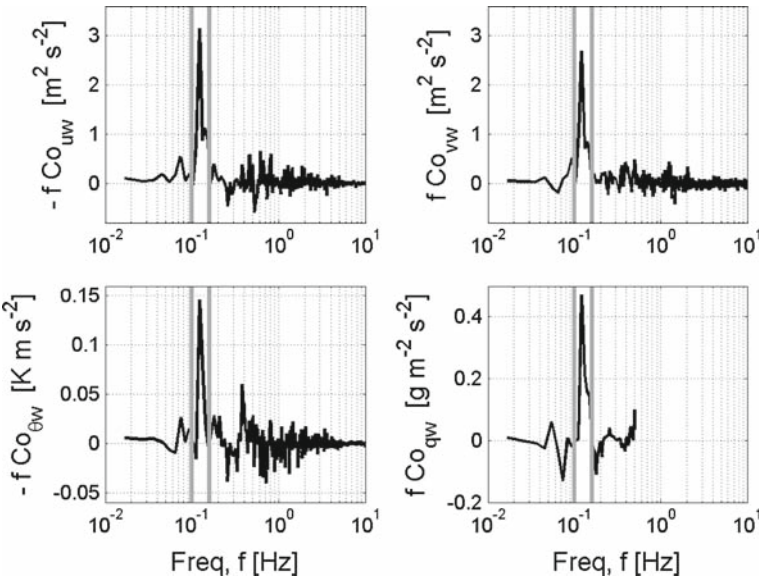

Fig. 9 For the cross-wind leg A, cospectra of the vertical velocity w with the horizontal wind velocity components u and v, potential temperature and humidity. The vertical grey lines indicate the roll-frequency band

of SST for water vapour path and reflected radiation have been made according to Drennan et al. (2007).

From Fig. 7, all spectra from cross leg A have higher spectral densities in the frequency (f) band 0.1–0.16 Hz and peak at frequencies near 0.13 Hz. Similarly, the cospectra in Fig. 9 show significant peaks at nearly the same frequencies within 0.1–0.16 Hz, indicating a coherent roll structure. In contrast no such peaks are evident in spectra or cospectra from the along-wind or transverse wind runs, B–E. The peak frequencies within the band, which correspond to a roll wavelength of 900 m, show good agreement with the SAR measurements. Considering the boundary-layer height indicated by the potential temperature profile of 500 m, the aspect ratio of these rolls is about 1.8.

The influence of scale on the fluxes can be studied by dividing the covariance into three spectral regions: $f < 0.1$ Hz, $f = 0.1$–0.16 Hz and $f > 0.16$ Hz. The low-frequency band ($f < 0.1$ Hz) contains larger or mesoscale eddies, the roll-frequency band ($f = 0.1$–0.16 Hz) is dominated by roll vortices, and the high-frequency band contains smaller scale eddies and turbulence of the inertial subrange (Chou and Ferguson 1991). The cospectral plots in the lower panels of Fig. 9 (note the negative sign multiplying the $\theta' w'$ cospectrum) indicate a strong net downward transport of warmer dry air within the roll-frequency band. This indicates that roll circulations carry air parcels with q and θ highly negatively correlated, and therefore transfer sensible heat downward and moisture upward. The cospectra of sensible heat are positive with smaller magnitudes for the high frequency band, in agreement with the slightly unstable conditions indicated by the stability index z/L in Table 1.

In order to assess the contribution of rolls to the total air-sea fluxes, we show in Fig. 10 the cumulative cospectral sums or ogives (Friehe et al. 1991) for the along-wind and cross-wind components of momentum flux for the five flux runs A–E. Here the solid black line represents the cross-wind leg (A), the dashed black lines represent the near along-wind legs (B, C and D),

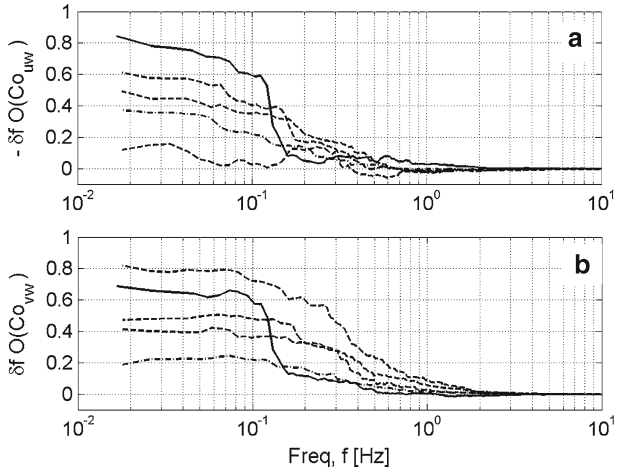

Fig. 10 Cumulative cospectral sums (ogives) of the along-wind (**a**) and cross-wind (**b**) components of the momentum flux for the NOAA43 boundary-layer flight. Here, the solid black line represents the cross-roll leg (A), the dashed black lines represent the three near-along-roll legs (B, C, and D), and the dash-dotted line represents the transverse-roll leg (E)

and the dash-dotted line represents the transverse wind leg (E). The top panel shows the stress in the mean wind direction (i.e., towards the aircraft for the along-wind flights, almost perpendicular to the aircraft track for the cross-wind flight); the bottom panel the stress in the cross-wind direction. In all cases, the flatness of the ogive curves at low and high frequencies indicates that energy-containing scales of the flux processes are well sampled.

The cross-wind run, leg A, stands out from the other curves in that the cumulative sum of both along-wind and cross-wind stresses is dominated by contributions from the roll frequency band. Indeed, over half the total flux from leg A originates in the relatively narrow roll band, compared with O(10%) for the other runs. This is consistent with the simulations of Glendening (1996), though well below the predictions of Morrison et al. (2005). The total stress of the cross-wind run is about 50% higher than the mean of the along-wind legs. We discuss this further below.

Figure 11a shows the ogives for the sensible heat flux of the five flux runs. Once again, the cross-wind leg A shows a dominant contribution to the covariance from the narrow roll frequency band, something not seen in the other legs. However, it is notable that the covariance heat flux for the cross-wind leg is nearly equal to the mean of that for the along-wind and transverse legs, indicating that the modulation by rolls of the sensible heat flux at the middle of the boundary layer is not as significant as with the momentum flux. It seems that the rolls redistribute the sensible fluxes among spatial scales without changing the total vertical transport.

5 Discussions and Conclusions

Results from an aircraft case study together with analysed SAR imagery have been presented. This is the first case of a confirmation by aircraft that the streaks seen in a SAR image are indeed roll vortices. The wavelengths of the roll features seen in the SAR images, about 900 m, agree well with those of features seen in the cross-wind flight leg. The boundary-layer

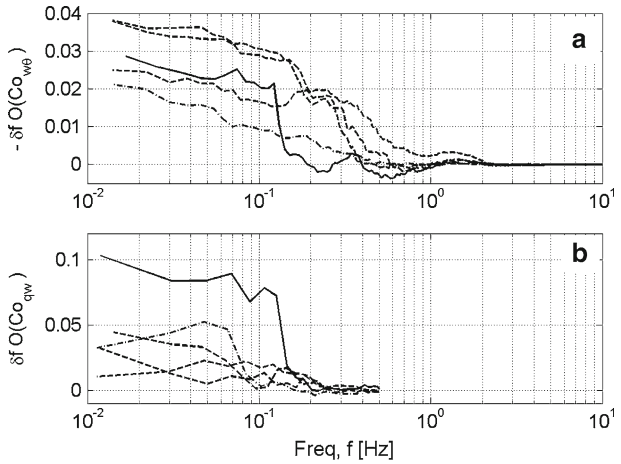

Fig. 11 Cumulative cospectral sums of the sensible heat (**a**) and humidity flux (**b**) for the 22 September 2002 NOAA43 boundary layer flight. Curves are as in Fig. 10. Note that the humidity data are measured by the chilled-mirror hygrometer at 1 Hz

height was estimated from GPS dropsondes to be around 500 m, giving an aspect ratio of the rolls about 1.8, which is in very good agreement with the result of Lorsolo et al. (2008).

One goal of this study was to quantify the contribution of boundary-layer rolls to the air–sea transport of momentum and heat. Previous studies have suggested that rolls contribute half (Glendening 1996) or considerably more (Morrison et al. 2005) of the total momentum flux, resulting in a strongly enhanced transfer when rolls are present. Our data analyses indicate the expected enhancements of rolls due to fluxes to be O(50%), consistent with Glendening (1996), but well below the estimates of Morrison et al. (2005) a result that might be expected given their overestimate of roll wavelength shown by Lorsolo et al. (2008).

While earlier research using both numerical models and observations has focused on surface stress (the momentum flux) in the hurricane boundary layer, little to date has been reported about the effect of rolls on the heat or humidity fluxes. In this work, the effect of rolls on the sensible heat flux was found to be small, more of a redistribution among scales than an enhancement. In the middle of the boundary layer, rolls tend to rescale eddies that transport heat flux.

We also show the high correlation of sensible heat and moisture at the roll scale in the cospectra plots. Given the asymmetry of the roll circulations postulated by Foster (2005), with much stronger and narrower updraft regions of rolls, we expect that the modulation of rolls on the humidity flux could be higher. As shown in Fig. 11b the humidity flux is about 150% higher for the cross-wind leg than for the mean of other flight legs, assuming that there is no significant difference for the humidity flux cospectra of these legs at frequencies higher than 0.3 Hz (unlikely). However, due to the lack of a fast response humidity sensor in the case study, the results for humidity flux are at best tentative.

To place these Hurricane Isidore data into context, we recall the recent results of French et al. (2007), who reported observations from Hurricanes Fabian and Isabel collected when these storms were major open ocean hurricanes (categories 4 or 5). Sampling was carried out in three of the four storm quadrants (omitting only the left rear), roughly 100–200 km from the storm centres. The French et al. study included a total of 48 'good' runs: 34 sampled along-wind, and 14 cross-wind. There was no evidence of boundary-layer rolls in any of

these data, but it was noted that the criteria used to select the cases may have eliminated some isolated rolls, especially in the along-wind runs. Eleven runs were rejected on the basis of poorly behaved ogives or cospectra. A subsequent wavelet reanalysis of these "bad" runs indicates the possible presence of boundary-layer rolls in only 2 of the 11 cases. However, given the large number of cross-wind runs in Hurricanes Isabel and Fabian with no evidence of rolls, it seems unlikely that boundary-layer rolls were present in these storms, at least at the locations sampled. Although there are no SAR images to corroborate this, we consider the Isabel and Fabian data of French et al. (2007). to be typical of conditions without boundary-layer rolls—or where rolls play an insignificant role.

The total stress of the cross-wind leg, where rolls were sampled, was found to be roughly 50% larger than that of the along-wind legs. However some of this enhancement can be attributed to differences in wind speed. By looking at the drag coefficient much of the variability due to wind speed is removed. For the four along-wind and transverse-wind legs here (B–E), where rolls are present in the SAR image, but not evident in the aircraft data, the mean drag coefficient C_{D10N} is $(2.04 \pm 0.12) \times 10^{-3}$, showing one standard deviation, which is not significantly different from the CBLAST average for similar wind speeds reported by French et al. (2007). For cross-wind leg A, where rolls were well sampled, $C_{\mathrm{D10N}} = 2.51 \times 10^{-3}$ about 20% higher than legs B–E and the CBLAST mean. This result is corroborated by results from the recent SOWEX study in the high wind regime of the Southern Ocean. While Chen et al. (2001) reported that rolls carried a significant fraction of the momentum flux during SOWEX, the SOWEX drag coefficients reported by Banner et al. (1999) were not enhanced over expected values. In fact they agree well with those reported here and by French et al. (2007). Moreover, the influence of rolls on the exchange coefficient of sensible heat flux is expected to be small given the uniform SST and boundary-layer environments indicated by the potential temperature profiles in Fig. 4 during the flux measurements. However the surface sensible heat flux and the exchange coefficient for heat can not be estimated for these runs due to the lack of stepped descent legs needed to extrapolate measured fluxes to surface values.

One obvious limitation of this work is the small amount of data (one flight) available to us. Although the intention was to coordinate aircraft flights with SAR overpasses, this proved difficult to achieve due to the relatively limited number of SAR overpasses, and to competing operational constraints on the flights. Unfortunately, the likelihood of future hurricane boundary-layer flights is now small, due to safety concerns following several recent incidents. The best possibilities for future HBL turbulence data would appear to lie with the use of remotely operated aircraft or sondes.

Finally we note the need for additional SAR imagery over tropical cyclones. At this point it remains unclear how frequently rolls occur in hurricanes. Most studies on rolls in the HBL to date, including this one, have focused on "landfalling" storms. It appears that rolls occur frequently in these conditions. However the CBLAST flights into Hurricanes Fabian and Isabel while in the open ocean failed to detect rolls. A larger data base of SAR imagery would help resolve this issue.

Acknowledgements We gratefully acknowledge support from ONR (N00014-01-F-0090) and NASA (W-19-835), as well as our collaboration with the CSA through the Hurricane Watch program. We appreciate the efforts of the many people involved in planning and carrying out CBLAST. We acknowledge in particular the efforts of Simon Chang and Carl Friehe (both formerly ONR), Jim Roles and Terry Lynch at NOAA AOC, Paris Vachon (CCRS) and Frank Marks (NOAA AOML). We also thank our CBLAST co-investigators as well as the many scientists, engineers and technicians at NOAA Aircraft Operations Center at MacDill AFB, Tampa, and NOAA AOML's Hurricane Research Division, along with the flight crew of NOAA43. We acknowledge Antonio Reppucci for help in analysing the SAR image, as well as Ralph Foster,

Sylvie Lorsolo and Mark Powell for their helpful comments. The lead author also acknowledges the support of National Research Council Research Associateship Award.

References

Alpers W, Brümmer B (1994) Atmospheric boundary layer rolls observed by the synthetic aperture radar aboard the ERS-1 satellite. J Geophys Res 99:12613–12621

Banner ML, Chen W, Walsh EJ, Jensen JB, Lee S, Fandry C (1999) The Southern Ocean Waves Experiment. Part I: overview and mean results. J Phys Oceanogr 29:2130–2145

Black PG, D'Asaro E, Drennan WM, French JR, Niiler PP, Sanford TB, Terrill EJ, Walsh EJ, Zhang JA (2007) Air-sea exchange in hurricanes: Synthesis of observations from the Coupled Boundary Layer Air-Sea Transfer experiment. Bull Amer Meteorol Soc 88:357–374

Brooks IM, Rogers DP (1997) Aircraft observations of boundary layer rolls off the coast of California. J Atmos Sci 54:1834–1849

Brown RA (1970) Secondary flow model for the planetary boundary layer. J Atmos Sci 27:742–757

Brown RA (1980) Longitudinal instabilities and secondary flows in the planetary boundary layer: a review. Rev Geophys Space Phys 18:683–697

Brümmer B (1999) Roll and cell convection in winter-time arctic cold-air outbreaks. J Atmos Sci 56: 2613–2636

Chen W, Banner ML, Walsh EJ, Jensen JB, Lee S (2001) The Southern Ocean Waves Experiment. Part II: sea surface response to wind speed and wind stress variations. J Phys Oceanogr 31:174–198

Chou S-H, Ferguson MD (1991) Heat fluxes and roll circulations over the Western Gulf Stream during an intense cold-air outbreak. Boundary-Layer Meteorol 55:255–282

Donelan MA (1990) Air-sea interaction. In: LeMéhauté B, Hanes D (eds) The sea, vol 9. Wiley-Interscience, pp 239–292

Drennan WM, Shay LK (2006) On the variability of the fluxes of momentum and sensible heat. Boundary-Layer Meteorol 119:81–107

Drennan WM, Zhang JA, French JR, McCormick C, Black PG (2007) Turbulent fluxes in the hurricane boundary layer, Part II: latent heat fluxes. J Atmos Sci 64:1103–1115

Etling D, Brown RA (1993) Roll vortices in the planetary boundary layer: a review. Boundary-Layer Meteorol 65:215–248

Farge M (1992) Wavelet transforms and their applications to turbulence. Annu Rev Fluid Mech 24:395–458

Foster RC (2005) Why rolls are prevalent in the hurricane boundary layer. J Atmos Sci 62:2647–2661

French JR, Drennan WM, Zhang JA, Black PG (2007) Turbulent fluxes in the hurricane boundary layer, Part I: Momentum flux. J Atmos Sci 63:1089–1102

Friedman KS, Vachon PW, Katsaros KB (2004) Mesoscale storm systems. In: Jackson CR, Apel JR (eds) Synthetic aperture radar marine users' manual. NOAA, Washington, DC, pp 331–340

Friehe CA, Khelif D (1992) Fast-response aircraft temperature sensors. J Atmos Oceanic Technol 9:784–795

Friehe CA, Shaw WJ, Rogers DP, Davidson KL, Large WG, Stage SA, Crescenti GH, Khalsa SJS, Greenhut GK, Li F (1991) Air-sea fluxes and surface turbulence around a sea surface temperature front. J Geophys Res 96:8593–8609

Glendening JW (1996) Linear eddy features under strong shear conditions. J Atmos Sci 53:3430–3449

Grossmann A, Morlet J (1984) Decomposition of Hardy functions into square integrable wavelets of constant shape. Siam J Math Anal 15:723–736

Horstmann J, Graber HC, Koch W, Iris S (2005) Investigation of SAR wind field retrieval with respect to hurricane winds. In: Proceedings of 2005 IEEE international geoscience and remote sensing symposium vol 6, 25–29 July 2005, pp 4018–4021

Katsaros KB, Vachon PW, Black PG, Dodge PP, Uhlhorn EW (2000) Wind fields from SAR: Could they improve our understanding of storm dynamics? Johns Hopkins APL Tech Dig 21:86–93

Katsaros KB, Vachon PW, Liu WT, Black PG (2002) Microwave remote sensing of tropical cyclones from space. J Oceanogr 58:137–151

Khelif D, Burns SP, Friehe CA (1999) Improved wind measurements on research aircraft. J Atmos Oceanic Technol 16:860–875

Koch W (2004) Directional analysis of SAR images aiming at wind direction. IEEE Trans Geosci Remote Sens 42:702–710

Laur H, Bally P, Meadows P, Schättler SJB, Lopinto E (1998) Derivation of the backscattering coefficient_0 in ESA ERS- 1/2.SAR.PRI data products. Technical Note ES-TN-RSPM- HL09, issue 2, Revision 5b, ESA, Frascati, Italy, 47 pp

Lehner S, Horstmann J, Koch W, Rosenthal W (1998) Mesoscale wind measurements using recalibrated ERS SAR images. J Geophys Res 103:7847–7856
Lehner S, Schulz-Stellenfleth J, Schättler JBH, Breit H, Horstmann J (2000) Wind and wave measurements using complex ERS-2 wave mode data. IEEE Trans Geosci Remote Sens 38:2246–2257
LeMone MA (1973) The structure and dynamics of horizontal roll vortices in the planetary boundary layer. J Atmos Sci 30:1077–1091
LeMone MA (1976) Modulation of turbulent energy by longitudinal rolls in an unstable boundary layer. J Atmos Sci 33:1308–1320
Levy G, Brown RA (1998) Detecting planetary boundary layer rolls from SAR. In: Brown RA (eds) Remote sensing of the Pacific Ocean by satellites. Earth Ocean and Space, pp 128–134
Li X, Pichel WG, He M, Wu SY, Friedman KS, Clemente-Colon P, Zhao C (2002) Observations of hurricane-generated ocean swell refraction at the Gulf Stream north wall with the RADARSAT-1 synthetic aperture radar. IEEE Trans Geosci Remote Sens 40:2131–2141
Lilly DK (1966) On the instability of Ekman Boundary Flow. J Atmos Sci 23:481–494
Lorsolo S, Schroeder JL, Dodge P, Marks F (2008) An observational study of hurricane boundary layer small-scale coherent structures. Mon Wea Rev (in press)
Morrison I, Businger S, Marks F, Dodge P, Businger JA (2005) An observational case for the prevalence of roll vortices in the hurricane boundary layer. J Atmos Sci 62:2662–2673
Mourad PD (1996) Inferring multiscale structure in atmospheric turbulence using satellite-based synthetic aperture radar. J Geophys Res 101:18433–18449
Mourad PD, Walter BA (1996) Viewing a cold air outbreak using satellite-based synthetic aperture radar and advanced very high resolution radiometer imagery. J Geophys Res 101:16391–16400
Mourad PD, Thompson DR, Vandemark D (2000) Extracting fine-scale wind fields from synthetic aperture radar images of the ocean surface. Johns Hopkins APL Tech Dig 21:108–115
Müller G, Brümmer B, Alpers W (1999) Roll convection within an Arctic cold-air outbreak: interpretation of in situ aircraft measurements and spaceborne SAR imagery by a three-dimensional atmospheric model. Mon Wea Rev 127:363–380
Nolan DS (2005) Instabilities in hurricane-like boundary layers. Dyn Atmos Oceans 40:209–236
Pasch RJ, Lawrence MB, Avila LA, Beven JL, Franklin JL, Stewart SR (2004) Atlantic hurricane season of 2002. Mon Wea Rev 132:1829–1859
Savtchenko S (1999) Effect of large eddies on atmospheric surface layer turbulence and the underlying wave field. J Geophys Res 104:3149–3157
Sikora TD, Ufermann S (2004) Marine atmospheric boundary layer cellular convection and longitudinal roll vortices. In: Jackson CR, Apel JR (eds) Synthetic aperture radar marine user's manual. NOAA, Washington, DC, pp 321–330
Stull RB (1988) An introduction to boundary layer meteorology. Kluwer Academic Publishers, Dordrecht, 666 pp
Uhlhorn EW, Black PG, Franklin JL, Goodberlet M, Carswell J, Goldstein AS (2007) Hurricane surface wind measurements from an operational stepped frequency microwave radiometer. Mon Wea Rev 9:3070–3085
Vachon PW, Katsaros KB (1999) Atmospheric cyclones from spaceborne SAR. Backscatter 10:14–19
Vandemark D, Mourad PD, Bailey SA, Crawford TL, Vogel CA, Sun J, Chapron B (2001) Measured changes in ocean surface roughness due to atmospheric boundary layer rolls. J Geophys Res 106:4639–4654
Weckwerth TM, Wilson JW, Wakimoto RM, Crook NA (1997) Horizontal convective rolls: determining the environmental conditions supporting their existence and characteristics. Mon Wea Rev 125:505–526
Wurman J, Winslow J (1998) Intense sub-kilometer boundary layer rolls in Hurricane Fran. Science 280: 555–557
Young GS, Kristovich DAR, Hjelmfelt MR, Foster RC (2002) Rolls, streets, waves, and more: A review of quasi-two-dimensional structures in the atmospheric boundary layer. Bull Amer Meteorol Soc 83: 997–1001